数理解析研究所講究録
1127巻 2000年 12-26

What generates the rhythm in a saline oscillator ?

名古屋大学大学院人間情報学研究科　岡村実奈　(Mina Okamura)
京都大学大学院理学研究科　吉川研一　(Kenichi Yoshikawa)

1 Introduction

In our environment, hydrodynamic flow accompanied with the time-dependent change of density is rather usual, see e.g., mixing of river stream with sea water and front movement in weather. Thus, it is very important to know the essentials in convection-diffusion system. However, even for the problem without diffusion or without density gradient, no analytical solution exists. In other words, the Navier-Stokes equation is not solvable even in the absence of density gradient, and is complex enough to induce various "unexpected" phenomena (e.g. chaos in Lorenz attractor). The aim of the present research is to obtain an intrinsic property buried in the "complexity" in convection-diffusion system, by picking up a curious phenomenon, so-called saline oscillator, as a simple convection-diffusion system.

The saline oscillator was discovered by Martin in 1970[1]. The experimental procedure is quite simple and the self-oscillatory behavior is highly reproducible. Fig.1(a) shows the experimental apparatus of the hydrodynamic oscillator. A plastic cup, with small orifice (ca. 1 mm diameter) in its base, filled with saline water, is placed within an outer vessel containing pure water. When the experiment starts at the point that the saline water level of the inner cup was nearly equal to that of the outer vessel, due to the imbalance of hydrostatic pressure, the saline water begins to flow downward. After a while, the down flow terminates, and then the pure water in the outer vessel begins to go upward through the orifice. This cycle repeats again and again (Fig.1(b)). This rhythmic phenomenon exhibits the characteristics of a nonlinear dynamical system. It has been subsequently shown that a saline oscillator exhibits various behaviors typical of a nonlinear oscillator; i.e. limit-cycle oscillation, bifurcation of the oscillatory mode and entrainment among oscillators[2-7]. If the essential aspects of such a visible nonlinear oscillator can be descried in simple mathematical terms, it should be helpful for understanding nonlinear rhythmic phenomena in physics, chemistry and biology. In the present study, we performed a numerical simulation on the curious periodic flow in a saline oscillator. The main purpose of this study was to

identify the essence of the mechanism of this oscillatory phenomenon through an analysis of the numerical simulation. In experimental studies, it is almost impossible to monitor time-dependant changes in the spatiotemporal structure, such as the velocity and energy dissipation at distinct points. On the other hand, a numerical study can provide detailed information on the spatiotemporal changes in various physical parameters.

2 Procedure for the Numerical Simulation

We performed a computer simulation of a saline oscillator with a three-dimensional flow field. We used the basic equations for an incompressible unsteady viscous fluid. Flow can be described by the Navier-Stokes equation, Eq.(1), and an equation of continuity, Eq.(2),

$$\frac{\partial \rho \boldsymbol{U}}{\partial t} + (\boldsymbol{U} \cdot \nabla)\, \rho \boldsymbol{U} = -\nabla P + \mu \nabla^2 \boldsymbol{U} + \rho \boldsymbol{g}, \tag{1}$$

$$\frac{\partial \rho}{\partial t} + \nabla \cdot (\rho\, \boldsymbol{U}) = 0, \tag{2}$$

where $\boldsymbol{U} = (u, v, w)$ is the velocity; P is the pressure; ρ is the density of the fluid; $\boldsymbol{g} = (0, 0, -g)$ is the gravitational acceleration; and μ is the coefficient of viscosity. Note that ρ is a spatiotemporal variable in our system, $\rho = \rho(x, y, z, t)$. For pratical purposes, the density of a fluid can be given as the sum of the density of water, ρ_0, and the density of salt, ρ_s. Thus, we evaluated the effects of density changes with the following equation of mass conservation, which includes the effect of diffusion,

$$\frac{\partial \rho_s}{\partial t} + \nabla \cdot (\rho_s \boldsymbol{U}) = D_s \nabla^2 \rho_s, \tag{3}$$

where ρ_s is the density of salt and D_s is the diffusion coefficient of salt.

We chose to use a cylindrical coordinate system with its origin at the center of the orifice with depth "d" and radius "a " (see Fig.2), so that r and z are the radial and vertical coordinates. We assume that the flow shows radial symmetry with respect to the vertical axis, and we use the Boussinesq approximation in the equations of motion. With this framework, the basic equations become

$$\begin{aligned} \frac{\partial u}{\partial t} &+ \frac{1}{r}\frac{\partial}{\partial r}(ru^2) + \frac{\partial}{\partial z}(uw) \\ &= -\frac{1}{\rho_0}\frac{\partial P}{\partial r} + \frac{1}{r}\frac{\partial}{\partial r}\left(2\nu r \frac{\partial u}{\partial r}\right) + \frac{\partial}{\partial z}\left(\nu\left(\frac{\partial u}{\partial z} + \frac{\partial w}{\partial r}\right)\right) - 2\nu\frac{u}{r}, \end{aligned} \tag{4}$$

$$\frac{\partial w}{\partial t} + \frac{1}{r}\frac{\partial}{\partial r}(ruw) + \frac{\partial}{\partial z}(w^2) = -\frac{1}{\rho_0}\frac{\partial P}{\partial z} + \frac{1}{r}\frac{\partial}{\partial r}\left(r\nu\left(\frac{\partial w}{\partial r} + \frac{\partial u}{\partial z}\right)\right) + \frac{\partial}{\partial z}\left(2\nu\frac{\partial w}{\partial z}\right) - \left(1 + \frac{\rho_s}{\rho_0}\right)g, \quad (5)$$

$$\frac{\partial u}{\partial r} + \frac{u}{r} + \frac{\partial w}{\partial z} = 0, \quad (6)$$

$$\frac{\partial \rho_s}{\partial t} + \frac{1}{r}\frac{\partial}{\partial r}(r\rho_s u) + \frac{\partial}{\partial z}(\rho_s w) = \frac{1}{r}\frac{\partial}{\partial r}\left(rD_s\frac{\partial \rho_s}{\partial r}\right) + \frac{\partial}{\partial z}\left(D_s\frac{\partial \rho_s}{\partial z}\right), \quad (7)$$

where u and w are the radial and vertical velocities, respectively; $\nu(=\mu/\rho_0)$ is the kinematic viscosity.

In addition to the above equations for fluid motion, we must also consider the effect of the free surface. For this purpose, we adapted the so-called Volume of Fluid method (VOF method)[8]. In this method, a function $F(x, y, z) = [0, 1]$ is defined as $F = 1$ for spatial elements fully occupied by fluid and $F = 0$ elsewhere. The summation of F over the entire system is constant and equals to the fractional volume of the cells occupied by fluid. The time dependence of F is governed by the following equation

$$\frac{\partial F}{\partial t} + \frac{1}{r}\frac{\partial}{\partial r}(rFu) + \frac{\partial}{\partial z}(Fw) = 0. \quad (8)$$

We performed calculations with the above equations using fluid-dynamic analysis software, FUJITSU/α-FLOW, provided by FUJITSU LIMITED[9]. The parameters and conditions for the numerical calculation were as follows.

The system consists of a cup with an orifice at the bottom and an outer vessel, as shown in Fig.2: the parameters are: $r_{in} = 2.25$ cm, $r_{out} = 5.0$ cm, $a = 0.05$ cm, $b = 0.25$ cm, $d = 0.1$ cm, $H_0 = 5.9$ cm. We divided the domain into 52×132 grids in the radial and vertical directions. To take into account the effect of the fluid dynamics near the orifice, the space within the orifice was divided into smaller grids, 5×4 in the radial and vertical directions, where the ratios of the maximum to minimum grid size are 10 and 4, respectively. The finite-difference approximation with a second-order central scheme was used to solve the basic equations, except for the convection term. For the convection term in Eqs.(4)(5) and (7), the QUICK scheme, which is a second-order accurate finite-difference method was

used[10]. The convection term in Eq.(8) was approximated by Donor-Acceptor method[11]. The slip boundary condition is taken for the velocity on the wall and the axis ($r = 0$), except for the wall within the orifice: the normal velocity component vanishes at the wall, and there is no gradient in tangential velocity. On the wall within the orifice, the boundary condition for the velocity is set to be non-slip: both normal and tangential velocities are always zero on the wall. The free-flux boundary condition is used to reflect the change in concentration.

3 Observation of the oscillator in real space

A saline oscillator was constructed with the following conditions, essentially the same as in the numerical simulation: $r_{in} = 2.25$ cm, $r_{out} = 5.78$ cm, $a = 0.05$ cm, $b = 0.25$ cm, $d = 0.1$ cm (see Fig.2). The initial amount of sodium chloride per unit volume in the cup was $\rho_s^0 = 0.11$ g/cm^3 in the initial condition, indicating that $\rho_{in} = 1.11$ g/cm^3, and $\rho_{out} = 1.0$ g/cm^3. The experiment was started with both of the initial heights, H_{in} and H_{out}, at about 5 cm. At first, the saline water begins to flow downward, and after approximately 1 minute, the downward flow stops. Soon after the fluid stops flowing around the orifice, the pure water in the outer vessel begins to flow upward through the orifice. This upward flow stops after several tens of seconds, and then the saline water again flows downward. This cycle repeats dozens of times. The period of oscillation is about 24 sec and stays almost constant; the periodicity increases less than 10 % even after a few hours on the experimental run.

Figure 3(a) shows a picture of the saline oscillator monitored with a CCD camera. In this Figure, saline water or pure water was colored by ink for visualization of the downward flow or upward flow, respectively. The change in the level of saline water in the inner cup was measured with a laser displacement meter (Keyence, LPB-02, Japan). The results are presented in Fig.4. From the amplitude of the rhythmic flow, it becomes clear that 0.12 % of the saline water flows out during each period.

4 Results of the Numerical Simulation

The numerical simulation was carried out with the following coefficients in the basic equations and initial conditions in Fig.2: $g = 980$, $\nu = 0.01$ cm^2/s, $\rho_s^0 = 0.1$ g/cm^3, $H_{in} =$

4.82cm, H_{out} = 4.99 cm. A small change in the initial height was shown to have no significant effect on the manner of oscillation. We have, thus, chosen a height difference so as to reduce the induction period before oscillation began. Under these initial conditions, saline water first began to flow downward, and upward flow began 70 sec later; i.e., oscillation began at this time. Figure 3(b) shows the spatial density profile of salt for the states with downward flow and upward flow. Figure 5(a), (b) shows the changes in the level of saline water in the inner cup, x, and the average velocity at the orifice, $\bar{w}$, where $\bar{w}$ is defined as

$$\bar{w} = \frac{2}{a^2 d} \int_{-d}^{0} \int_{0}^{a} w(r, z, t) r dr dz. \tag{9}$$

The period of oscillation was ca. 41 sec. Based on the change in the water level, it is found that 0.16 % of the saline water escaped from the cup during each period of oscillation. This may accord with 0.12 % in the corresponding experiment. In the simulation, as an artifact we noticed that, during the upward flow in each period of oscillation, the amount of salt in the inner cup increased by 0.001g, which is considered to have a negligible effect on the manner of the oscillation in the simulation.

5 Discussion

As shown above, our numerical simulation reproduced the experimental trend rather well, except for the difference in the period of oscillation; T = 24 sec in the experiment and T= 41 sec in the simulation. In our actual experiment with the saline oscillator, there is a small but finite irregularity around the fringe of the orifice. Such an irregularity could disturb the laminar flow around the orifice, which would influence the periodicity. Actually, we have confirmed that little modification on the shape of the orifice (for example, by making the periphery of the orifice smoother) induces the lengthening of the periodicity by 30 $\sim$ 50 %. In addition to such experimental problem, there are also some factors in the numerical simulation which particularly affect the periodicity, such as the size and arrangement of the grids and the boundary conditions. However, taking into account these factors in both the experiment and the simulation, the difference in periodicity is not considered to be a serious matter.

In Fig.4, the broken lines are depicted as single exponential, together with the experimental traces on the height of the level of the saline water. From this, it is clear that individual

periods both on upward flow and downward flow is interpreted well with first-order linear differential equation as in Eq.(10).

$$\dot{x}(t) = -kx(t) \quad (k > 0). \tag{10}$$

The next problem is how to interpret the process of the switching of the flow direction. Let us consider the critical hydrostatic pressure required to stop the downward flow of saline water and to initiate the upward flow of pure water. Based on the conservation of the total fluid volume, the changes in the heights of saline and pure water, Δh and $\Delta h'$, are related to each other by the ratio of the surface areas in the inner cup and the outer vessel, S_{in} and S_{out}.

$$\Delta h' = -\frac{S_{in}}{S_{out}}\Delta h. \tag{11}$$

The initial equilibrium height, H_{eq}^0 is given by

$$H_{eq}^0 = H_{in} - \Delta h, \tag{12}$$

where Δh is obtained from the following equation

$$(\rho_s^0 + \rho_0)g(H_{in} + \frac{d}{2} + \Delta h) = \rho_0 g(H_{out} + \frac{d}{2} + \Delta h'). \tag{13}$$

From Eq.(13), H_{eq}^0 is calculated to be 4.59 cm in the first cycle of the oscillation. As we mentioned in the preceding section, the density difference decreases with oscillatory flow. By denoting ΔH_{eq} as the difference between successive oscillations, the equilibrium height of the nth oscillation, $H_{eq}(n)$ is given by

$$H_{eq}(n) = H_{eq}^0 + (n-1)\Delta H_{eq}. \tag{14}$$

From the result of the numerical simulation, ΔH_{eq} is calculated to be 1.68×10^{-4} cm. By adapting a "moving axis", as $\Delta x = x - \Delta H_{eq}(n)$, the limit-cycle behavior represented by Δx vs. $\bar{w}$, is given as in Fig.6, where $\bar{w}$ is the average fluid velocity at the orifice and the interval between the data points is 0.1 sec. The cycles change as $A \to A' \to B \to B' \to A$. The temporal changes in the water level, and the average velocity and acceleration at the orifice are given in Fig.5(a),(b),(c). The flow accelerates upward in $A \to A'$, and decelerates during $A' \to B$. In $B \to B'$, upward flow stops and downward flow accelerates. In $B' \to A$,

downward flow decelerates. Here, the periods on $A \rightarrow A'$ and $B \rightarrow B'$ are shorter than 0.5 sec, corresponding to the process in the exchange of fluid within the orifice, from saline water to pure water and vice versa, respectively. As the switching of the flow is almost abrupt, the magnitude of the acceleration at the moment of the change in flow direction are two orders as large as that during one-directional flow through the orifice as is clear in the result of our simulation. If we carefully examine the switching process, it is apparent that just after the stop of the downward flow of saline water, pure water rises upward through the orifice from its edge, and this upward flow then accelerates. Except for the "moment" of the switching of the flow, the height exhibits single-exponential curve in the simulation, corresponding well to the present of the experiment (Fig.5 (a)).

To characterize the manner of the fluid motion, let us estimate the Reynolds number in the saline oscillator.

$$Re = \frac{\rho \bar{w} l}{\mu}, \tag{15}$$

where the density ρ of the fluid has a value between 1.0 and 1.1 g/cm^3, the characteristic length l ($l = 2a$) is 0.1 cm, and $\bar{w}$ is at the most 1.9 cm/sec, as shown in Fig.5. Thus, the maximum Reynolds number is no more than 20. This suggests that the effect of turbulence is almost negligible in this phenomenon.

Let us now examine the manner of the periodic flow using cylindrical coordinates. In the simulation, we have adopted the radial symmetry with respect to the vertical axis. We think that the numerical simulation on the approximation with radial symmetry may be almost satisfactory to describe the oscillator, at least on the switching between upward and downward flow. The driving force is considered to consist of four components; convection f_{con}, and the gradients of pressure f_{pre}, viscosity f_{vis}, and gravity f_{gra}. The effects of acceleration can therefore be described as follows:

$$\frac{\partial w}{\partial t} = f_{con} + f_{pre} + f_{vis} + f_{gra}, \tag{16}$$

$$f_{con} = -\frac{1}{r}\frac{\partial}{\partial r}(ruw) - \frac{\partial}{\partial z}(w^2), \tag{17}$$

$$f_{pre} = -\frac{1}{\rho_0}\frac{\partial P}{\partial z}, \tag{18}$$

$$f_{vis} = \frac{1}{r}\frac{\partial}{\partial r}\left(r\nu\frac{\partial w}{\partial r}\right) + \frac{1}{r}\frac{\partial}{\partial r}\left(r\nu\frac{\partial u}{\partial z}\right) + \frac{\partial}{\partial z}\left(2\nu\frac{\partial w}{\partial z}\right), \tag{19}$$

$$f_{gra} = -g - \frac{\rho_s}{\rho_0}g. \tag{20}$$

By integrating Eq.(16) over the entire volume in the orifice, the net driving force is given as in Eq.(21).

$$\begin{aligned}\frac{2}{a^2 d}\int_{-d}^{0}\int_{0}^{a}\frac{\partial w}{\partial t}r\,dr\,dz &= \frac{2}{a^2 d}\int_{-d}^{0}\int_{0}^{a}(f_{con}+f_{pre}+f_{vis}+f_{gra})r\,dr\,dz \\ &= F_{con}+F_{pre}+F_{vis}+F_{gra}.\end{aligned} \tag{21}$$

Figure 7 shows the temporal changes in the different components, $F_{pre}+F_{gra}, F_{vis}, F_{con}$, which accompany periodic flow in the saline oscillator, as deduced from the numerical simulation. Based on this figure, F_{con} and F_{vis} always have the role to depress the oscillation, and $F_{pre}+F_{gra}$ accelerates the flow. Figure 8(a)(b)(c) shows the change of the respective term, F_{con}, F_{vis}, $F_{pre}+F_{gra}$, at intervals of 0.1 sec as in Fig.6. From this Figure, it is clear that all terms, F_{con}, F_{vis} and $F_{pre}+F_{gra}$ are proportional to the average velocity, $\bar{w}$, except the moment of flow switching. During the continuous upward flow and downward flow, the coefficients of F_{con} and F_{vis} are negative and the coefficient of $F_{pre}+F_{gra}$ is positive. The summation of these contributions is negative.

$$\frac{d\bar{w}}{dt} = -k\bar{w} \quad (k>0). \tag{22}$$

This result explains why the profile of the water level in inner cup, x, is expressed by the profile $x(t) \propto e^{-kt}$. The period is, thus, determined by the competition between the pressure gradient and damping effect such as viscosity, as we mentioned before.

From the above results and discussion, it becomes evident that the dynamical behavior is interpreted with different characteristic stages between the continuous upward or downward flow, and the switching of the flow. Then, let us discuss further on the mechanism of the switching. Based on Fig.8(a), it is apparent that F_{con} is negligibly small compared to other components. As for the change in F_{vis}, we have noticed that the first term in Eq.(19), accounts for 96 % of F_{vis}; thus, the second and third terms are negligible. We also noticed that the flow profile at the orifice could be represented almost perfectly with a

parabola. In fact, there was actually only slight deviation from ideal Hagen-Poiseuille flow. By introducing a correction factor ε to Hagen-Poiseuille flow, F_{vis} can be represented as

$$F_{vis} = -\frac{8\nu}{a^2}\varepsilon\bar{w}. \tag{23}$$

By comparison with the results of the simulation, ε was determined to be $\varepsilon = 0.94$. Thus, the deceleration of the flow can almost be characterized by the first term in F_{vis}. Then, let us now discuss the pressure term in detail. We divide the pressure on both sides of the orifice, $z = 0, -d$ into hydrostatic pressure and the difference from it, $P^*(z)$. $P^*(z)$ corresponds to the effects of the discontinuous density distribution and the velocity of the flowing fluid.

$$P(0) = (\rho_s^0 + \rho_0)gx + P^*(0), \tag{24}$$

$$P(-d) = \rho_0 g(x' + d) + P^*(-d), \tag{25}$$

where x' is the level of pure water from $z = 0$ in the outer vessel and

$$x' = -\frac{S_{in}}{S_{out}}x + \left(\frac{S_{in}}{S_{out}}H_{in} + H_{out}\right). \tag{26}$$

Using the above expression, F_{pre} becomes

$$\begin{aligned} F_{pre} &= -\frac{1}{\rho_0}\frac{P(0) - P(-d)}{0 - (-d)} \\ &= \frac{P^*(-d) - P^*(0)}{\rho_0 d} - \frac{(\rho_0 + \rho_s^0)gx - \rho_0 g(x')}{\rho_0 d} + g. \end{aligned} \tag{27}$$

We can obtain the second term as a function of x strictly and the third term is canceled by the first term of F_{gra}. We use the expression F^*_{pre}, F^*_{gra} as the first term of F_{pre} and the second term of F_{gra}. Figure 8(d)(e) show F^*_{pre} versus $\bar{w}$ and F^*_{gra} versus $\bar{w}$, as in Fig.6. The interval between the data points is 0.1 sec. Based on the results of the simulation, the characteristics on F^*_{pre} woule be expressed as Eq.(28) with the symmetry of cubic function.

$$F^*_{pre} = \bar{w} - 30\bar{w}^3. \tag{28}$$

As shown in Fig.8(e), F^*_{gra} is represented as signum function with a good approximation.

$$F^*_{gra} = -\frac{\rho_s^0 g}{2} + \frac{\rho_s^0 g}{2}sgn(\bar{w}). \tag{29}$$

From the definition, $\bar{w}$ is given as

$$\bar{w} = \left(\frac{r_{in}}{a}\right)^2 \frac{\partial x}{\partial t}. \tag{30}$$

As $x(t)$, the level of saline water, is almost independent on the position, r, it may be allowed for us to adapt an ordinary differential instead of the partial differential in the above equation,

$$\frac{\partial x}{\partial t} \to \frac{dx}{dt}. \tag{31}$$

For the above the consideration, Eq.(21) becomes as follows with the substitution of X to $x - H_{eq}$

$$\frac{d^2X}{dt^2} = -A\left(1 + B\left(\frac{dX}{dt}\right)^2\right)\frac{dX}{dt} - \omega_0^2 X + \frac{\rho_s^0 g}{2} sgn(\bar{w}) + C, \tag{32}$$

where A, B, C, ω_0 are positive constants. It is worthy to notice that the first term is always negative. On this differential equation without the constant and signum function, the system becomes a damped oscillator, because ω_0^2 is larger than the square of the coefficient of $\bar{w}$. The limit cycle is, thus, maintained by the repetitive sudden change in the sign of the velocity.

From the characteristics given in Fig.8(f), the essential feature is represented with polynomial expansion through numerical fitting.

$$F_{pre}^* + F_{gra}^* = -51 + 90\bar{w} - 30\bar{w}^3 + \mathcal{O}(\bar{w}^4). \tag{33}$$

Thus Eq.(21) can be rewritten as

$$\frac{d^2X}{dt^2} = 56\frac{dX}{dt} - 1.2 \times 10^8 \left(\frac{dX}{dt}\right)^3 - 7X. \tag{34}$$

Interestingly, this ordinal differential equation corresponds to the a so-called Layleigh equation [6,7]:

$$\frac{d^2X}{dt^2} = \tilde{A}\frac{dX}{dt} - \tilde{B}\left(\frac{dX}{dt}\right)^3 - \omega_0^2 X, \tag{35}$$

where $\tilde{A}, \tilde{B}, \omega_0^2$ are positive constants. The Layleigh equation implies the following physical meaning; the third term on the right together with the left second time-derivative constitutes an oscillator, and the first and second terms on the right correspond to "negative"

and positive friction, respectively. In the actual saline oscillator, X is the fluid level from the equilibrium height, and ω_0^2 corresponds to Eq.(36) as is deduced from Eqs. (21), (26), (27)

$$\omega_0^2 = -\frac{g}{d}\left(\frac{a}{r_{in}}\right)^2\left(1+\frac{S_{in}}{S_{out}}+\frac{\rho_s^0}{\rho_0}\right). \tag{36}$$

As have been shown both on the simulation and the experiment, the system is "energized" due to the sudden change in the "effective mass" of the flow. Such an abrupt energization, or the process of switching, exhibits the odd symmetry with respect to the fluid velocity. Thus, such an effect can be most simply represented as the cubic function of the velocity as in the second term on the right side in the layleigh equation, Eq.(35).

In the saline oscillator, energy is stored as gravitational instability where the high-density saline water is situated above the low density of pure water. We took the potential energy of a discrete fluid cell as

$$U(i,k) = \rho(i,k)\Delta V(i,k)gh(i,k), \tag{37}$$

where i and k are the grid numbers in the horizontal and vertical directions, respectively, and reflect the position of the cell. $\rho(i,k) = \rho_0 + \rho_s(i,k)$ is the density of the cell, $\Delta V(i,k)$ is the volume of the cell and $h(i,k)$ is the height from the bottom of the outer vessel. By summing Eq.(37) over the entire fluid, the net potential energy can be evaluated. The stored potential energy in the saline water in the inner cup is, thus, calculated to be 2×10^3 [g·cm^2/s^2], compared to that in the final state where the fluid exhibits a uniform density and the fluid levels in the inner cup and the outer vessel are the same. Each oscillation consumes 0.08 % of this stored energy: where 78 % of the consumed energy is converted into kinetic energy and the rest is dissipated by viscosity.

The conclusion that the essence of the saline oscillator can be described with a Layleigh equation is consistent with previous findings on coupling between saline oscillators[4,7-8]; i.e., when two cups of saline water with orifices are situated in a same outer vessel of pure water, the rhythmic flows self-synchronize in an exact antiphase mode. This curious behavior has been successfully interpreted by coupled Layleigh equations, at least phenomenologically. Thus, the present study provides a theoretical basis for why the coupling between saline oscillators can be rather well simulated with coupled Layleigh equations.

References

[1] S. Martin, Geophys. Fluid Dyn. **1,** 143 (1970).

[2] K. Yoshikawa, S. Maeda, and H. Kawakami, Ferroelectrics **86,** 281 (1988).

[3] K. Yoshikawa, S. Nakata, M. Yamanaka, and T. Waki, J. Chem. Edu. **66,** 205 (1989).

[4] K. Yoshikawa and K. Fukunaga, Chem. Phys. Lett. **174,** 203 (1990).

[5] K. Yoshikawa, N. Oyama, M. Shoji, and S. Nakata, Am. J. Phys. **59,** 137 (1991).

[6] K. Yoshikawa and Y. Murofushi, Forma **5,** 83 (1990).

[7] S. Nakata, T. Miyata, N. Ojima, and K. Yoshikawa, Physica D **115,** 313 (1998).

[8] B. D. Nichols, C. W. Hirt and R. S. Hotchkiss, *Los Alamos Scientific Lab.* **LA-8355** (1980).

[9] *FUJITSU/α - FLOW Technical manual* (in Japanese), (FUJITSU LIMITED, 1992). Information on the software package is available from http://www.atip.or.jp/public/atip.reports.91/alpha.html.

[10] B.P.Leonard, *Comput. Method Appl. M.* , **19,** 59 (1979).

[11] W. E. Johnson, Systems, Science and Software report 3SR-353 (1970).

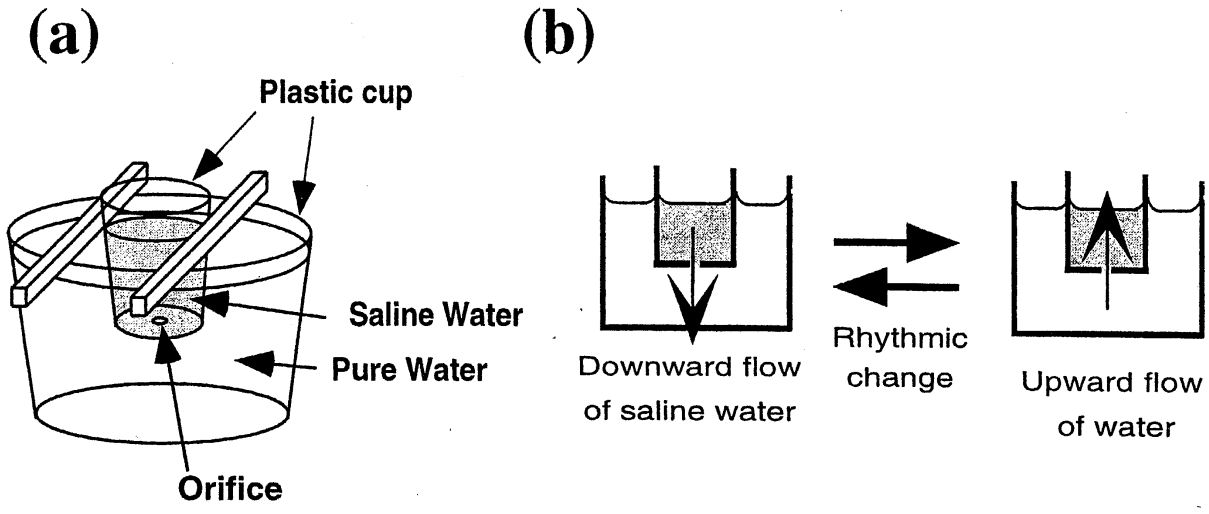

Figure 1: (a) Experimental apparatus for the saline oscillator. The outer vessel and the inner cup are filled with pure water and saline water, respectively. (b) Schematic representation of oscillatory flow in the saline oscillator.

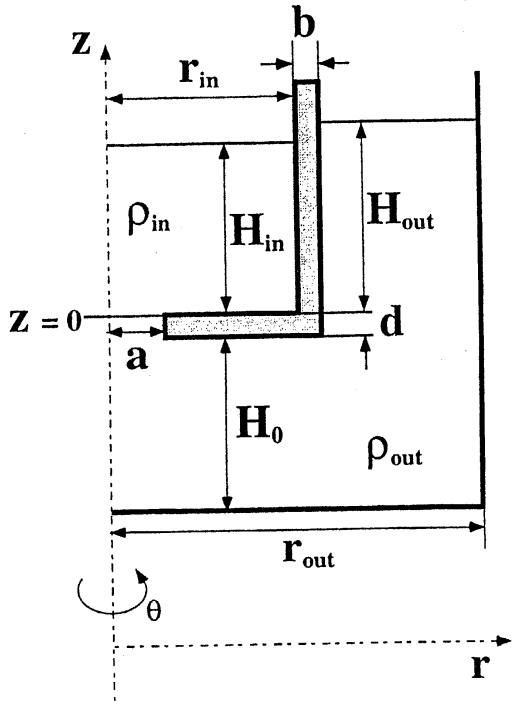

Figure 2: Coordinates in the saline oscillator. r and z are the radial and vertical coordinates.
r_{in} : inner radius of the cup, r_{out} : radius of the outer vessel, a : radius of the orifice, b : thickness of the inner cup, d : depth of the orifice, $\rho_{in}(=\rho_0+\rho_s^0)$: initial density in the cup, $\rho_{out}(=\rho_0)$: initial density of the outer vessel , H_{in} : initial height of saline water, H_{out} : initial height of pure water, H_0 : depth of the outer vessel. Here ρ_s^0 is the initial amount of sodium chloride per unit volume in the cup and ρ_0 is the density of pure water.

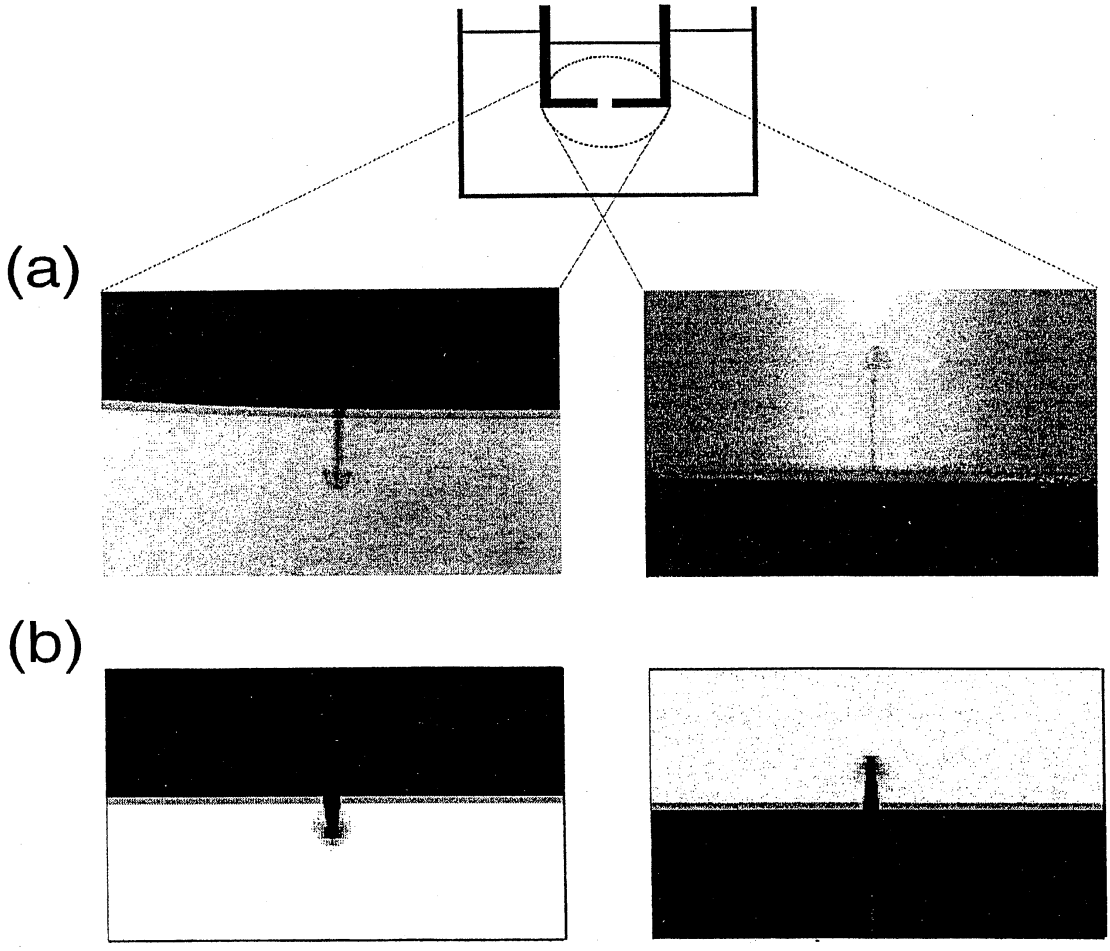

Figure 3: Flow profile in the saline oscillator for the down-stream of saline water (left) and the up-stream of pure water (right). (a) An actual experiment in the saline oscillator with r_{in} = 2.25 cm, r_{out} = 5.78 cm, a = 0.05 cm, b = 0.5 cm, d = 0.1 cm, and ρ_s^0 =0.11 g/cm^3. Saline water or pure water was colored by ink for visualization of the downward flow or upward flow, respectively. (b) Computer simulation of the saline oscillator with r_{in} = 2.25 cm, r_{out} = 5.0 cm, a = 0.05 cm, b = 0.5 cm, d = 0.1 cm, and ρ_s^0=0.1 g/cm^3. See Fig. 2 for abbreviations.

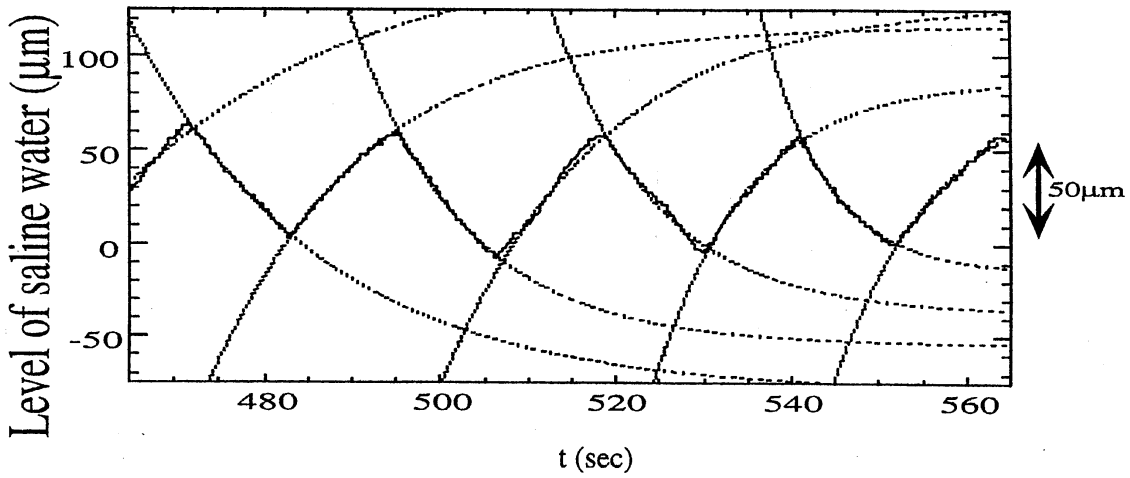

Figure 4: Experimental results on the rhythmic change in the level of saline water in the inner cup. The broken lines represent single exponential fits for the individual stages, during the upward flow and the downward flow: $x(t) \propto e^{-kt} + const.$

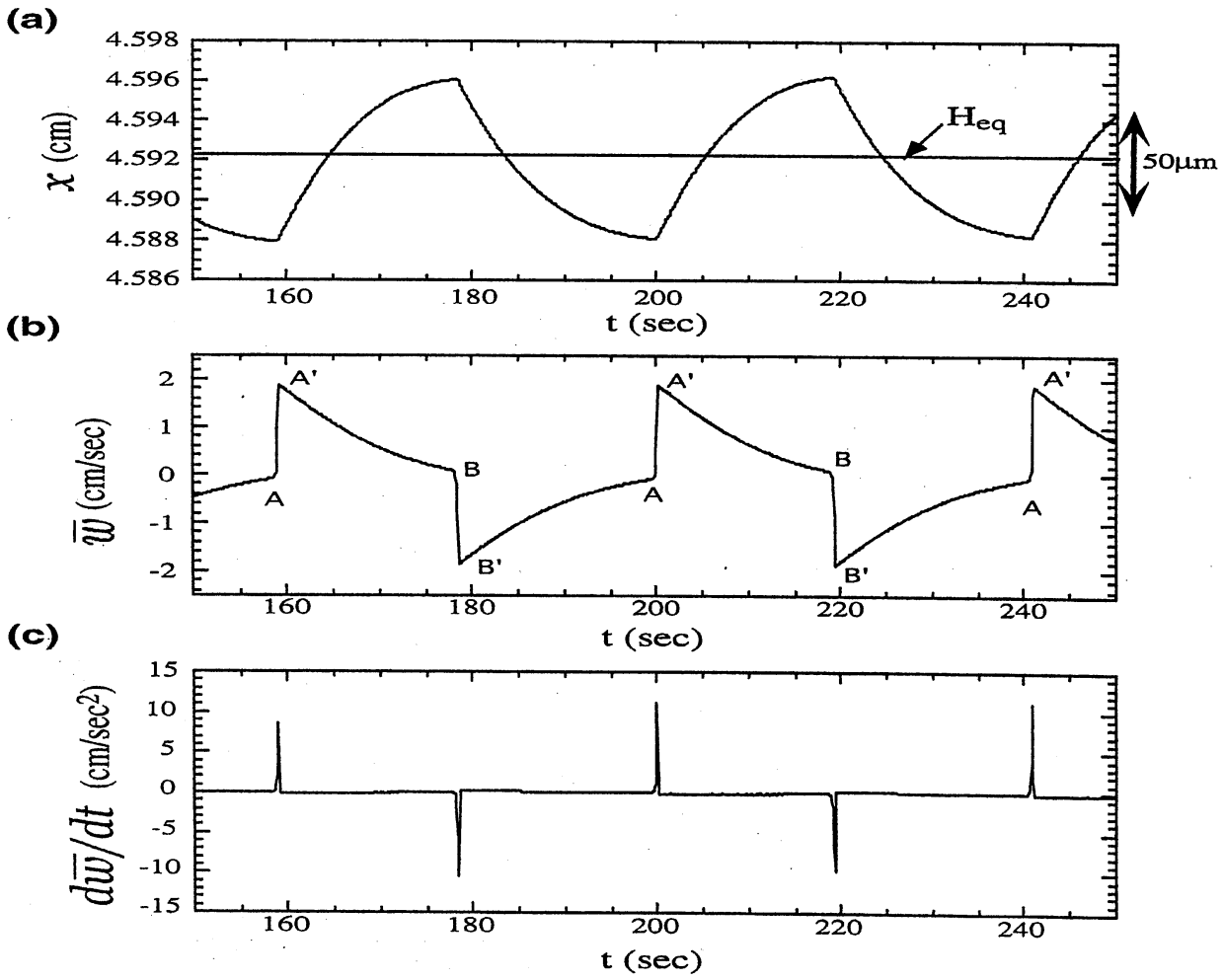

Figure 5: (a) Numerical simulation of the change in the level of saline water in the inner cup, x. The broken line shows the equilibrium height ($H^0_{eq} = 4.59cm$) where the inner and outer hydrostatic pressures are equal at the center of the orifice; $z = -d/2$. (b) The average velocity at the orifice, $\bar{w}$. (c) The acceleration at the orifice, $d\bar{w}/dt$.

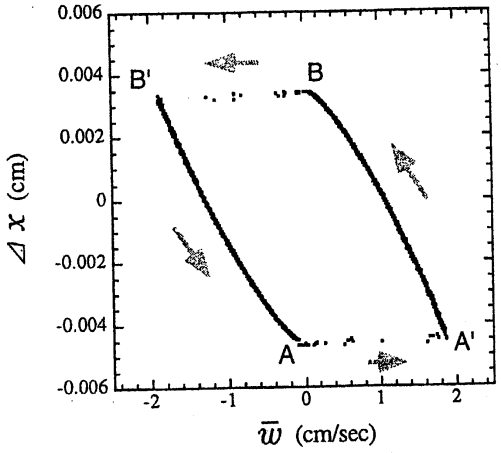

Figure 6: Numerical simulation of the limit-cycle behavior in the saline oscillator shown as Δx vs. $\bar{w}$, where $\Delta x = x - H_{eq}(n)$ and $\bar{w}$ is the average velocity at the orifice. The interval between the data points is 0.1 sec.

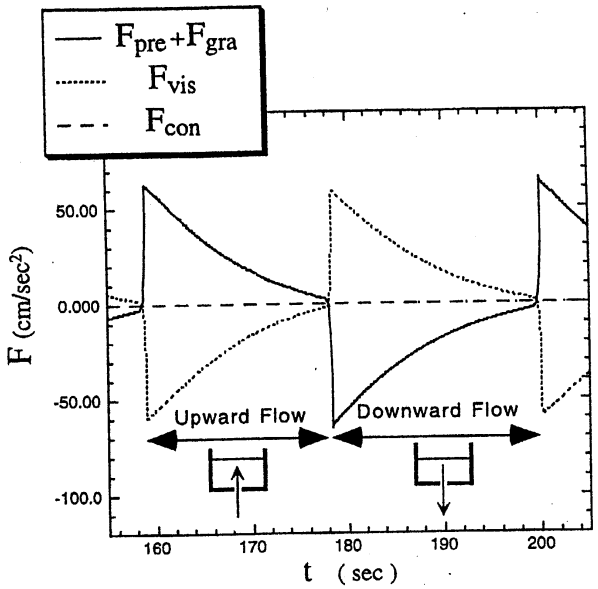

Figure 7: Time-dependent change in the individual components of the force needed to induce acceleration in fluid flow. F_{con} is the convection term, F_{pre} is the pressure term, and F_{vis} is the viscosity term, and F_{gra} is the gravity term.

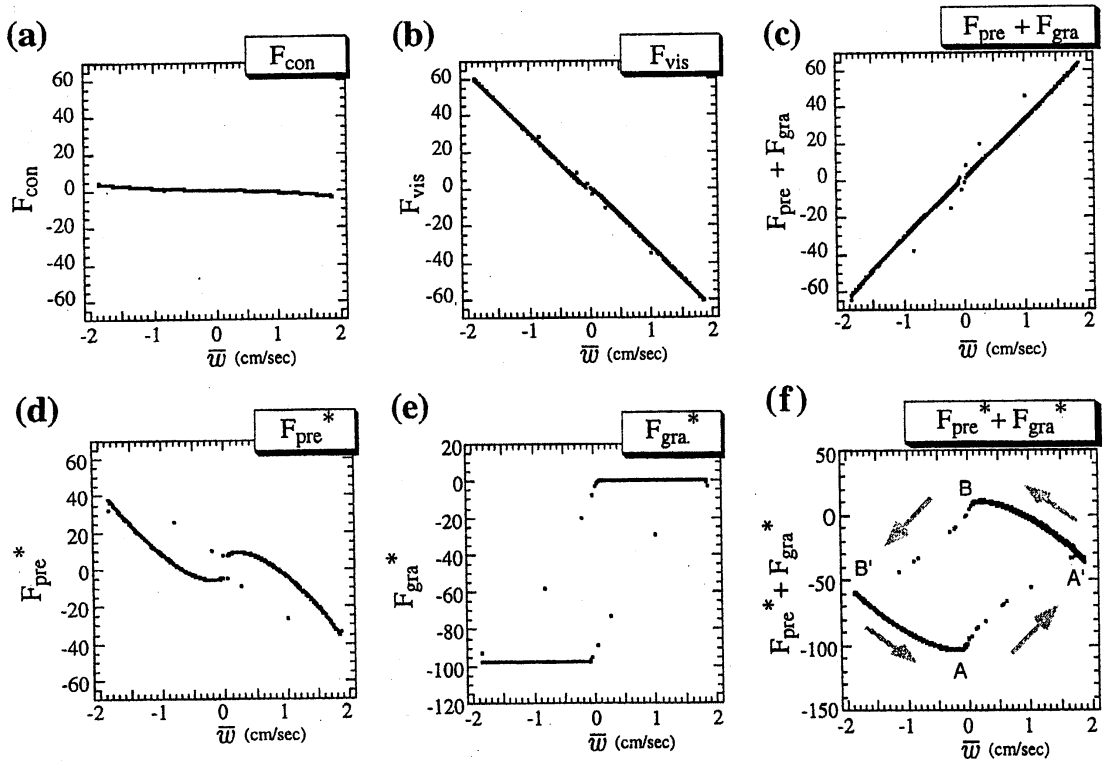

Figure 8: (a) Phase portrait of $F_{con}(cm/sec^2)$ with respect to the average velocity, $\bar{w}(cm/sec)$, at the orifice. (b) Phase portrait of $F_{vis}(cm/sec^2)$ with respect to the average velocity, $\bar{w}(cm/sec)$, at the orifice. (c) Phase portrait of $F^*_{pre} + F^*_{gra}(cm/sec^2)$ with respect to the average velocity, $\bar{w}$, at the orifice. (d) Phase portrait of $F^*_{pre}(cm/sec^2)$ with respect to the average velocity, $\bar{w}(cm/sec)$, at the orifice. (e) Phase portrait of $F^*_{gra}(cm/sec^2)$ with respect to the average velocity, $\bar{w}(cm/sec)$, at the orifice. (f) Phase portrait of $F^*_{pre} + F^*_{gra}(cm/sec^2)$ with respect to the average velocity, $\bar{w}(cm/sec)$, at the orifice. The interval between the data points is 0.1 sec.